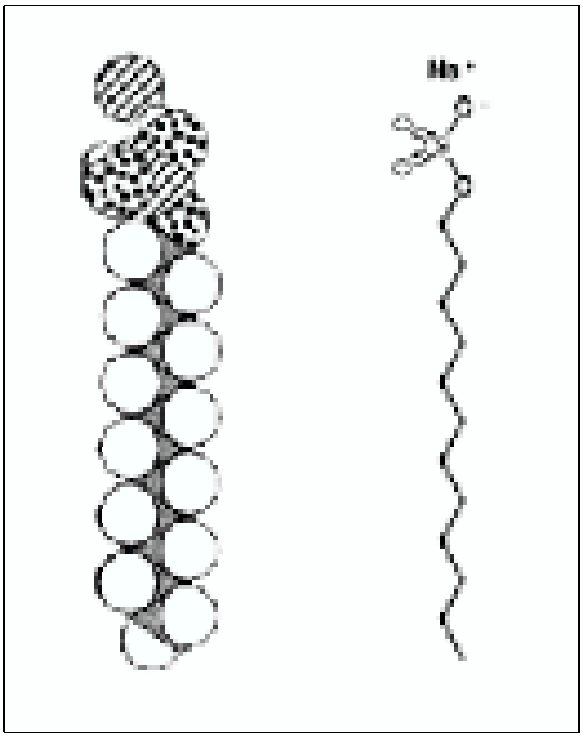

Figure 1: Sodium dodecyl sulphate (SDS) is the soap in your shampoo.

Case Study: Scattering from membrane-based phases

Amphiphilic molecules

Amphiphilic molecules are molecules containing (at least) two moities which have very different affinities. For example, SDS, shown in Fig. 1, has a aliphatic chain that has a high affinity for oil (alkane), chemically-bonded to an ionic group that has a high affinity for water. Similarly for lecithin.

As a consequence, as shown in Fig. 4 binary or tertiary mixtures of oil-water-amphiphile *self-assemble* into more-or-less elaborate structures, which have the role, *e.g.* in the case of SDS/water of protecting the aliphatic chains from water, which in that case, they do by forming micelles.

The molecular geometry (which may be temperature dependent) is key in determining the morphology of self-organiztion. Thus, while SDS, with one

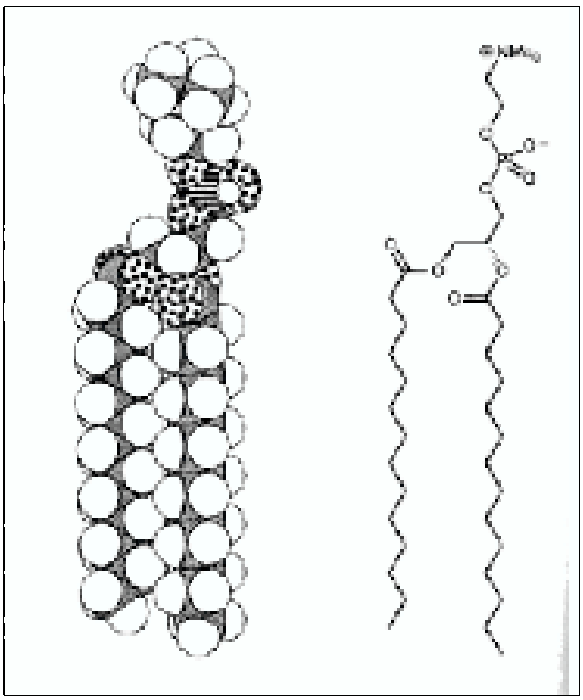

Figure 2: Lecithin is a lipid, similar to those that make up the membranes surrounding your cells.

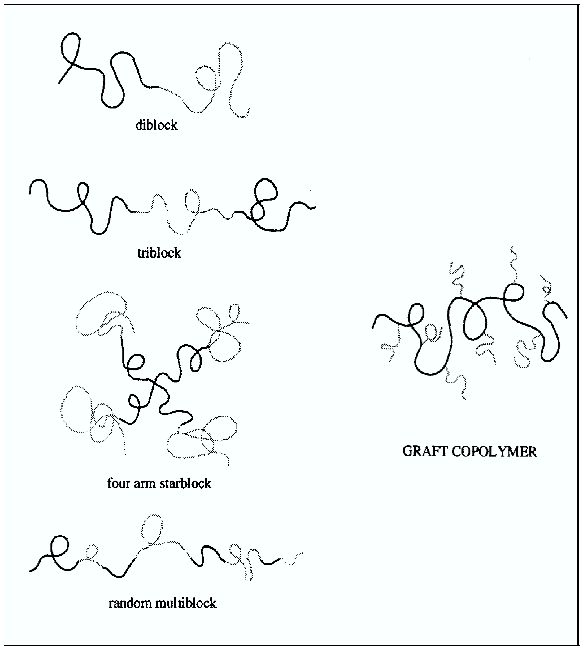

Figure 3: Block copolymers are amphiphilic because chemically different polymers (usually) do not like to mix, because polymers have relatively little entropy of mixing.

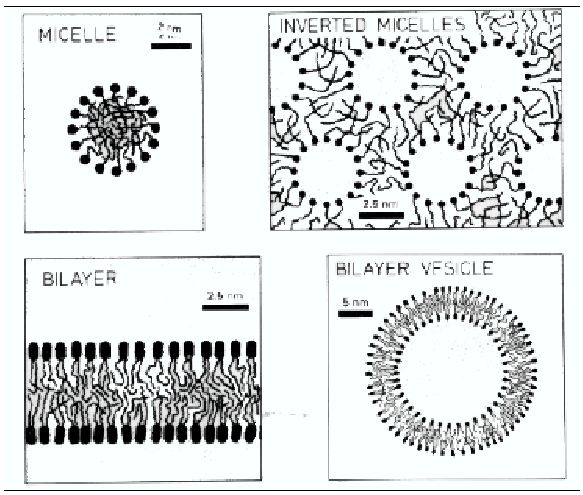

Figure 4: Various self-assemble structures in binary (solvent-amphiphile) mixtures.

aliphatic chain, forms spherical micelles in water, lecithin, with two chains similarly-long aliphatic chains forms extended bilayer membranes.

Phase diagrams

Fig. 5 [Strey et al.(1990)Strey, Shomaker, Doux, Nallet, and Olsson, Roux et al.(1992)Roux, Coul shows the phase diagram of $C_{12}E5$ – a non-ionic surfactant (*a.k.a.* non-ionic amphiphile) in water, plotted on a semilogarithmic scale to emphasize the behavior at low surfactant concentrations. There are several different phases:

- The L_1 phase consists of $C_{12}E_5$-micelles in water.
- The L_2-phase is a reverse micelle phase, consisting of spheres of water in $C_{12}E_5$.
- The L_α phase is a lamellar phase, in which the amphiphiles self-organized into bilayers, with the hydrophobic moieties protected within the interior of the bilayer, and in which the bilayers themselves self-organize into an ordered, periodic structure, with the symmetry of a SmA liquid crystal. item The L_3 phase, which we focus on in this presentation, is also a phase consisting of bilayer membranes, but in this case the membranes take on a randomly-connected, disordered morphology.

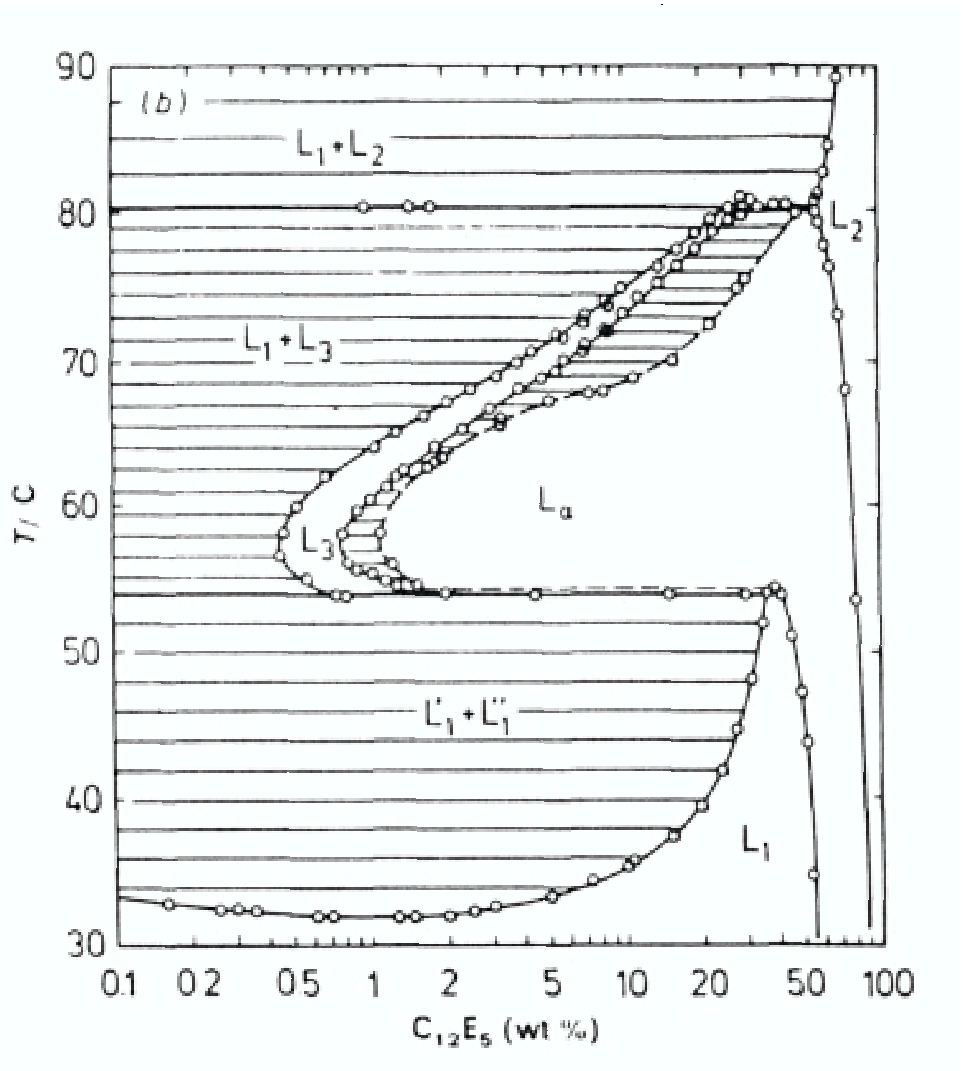

Figure 5: $C_{12}E_5$-water phase diagram *vs.* temperature and wt% $C_{12}E_5$. Two phase regions are lined. One phase regions are clear.

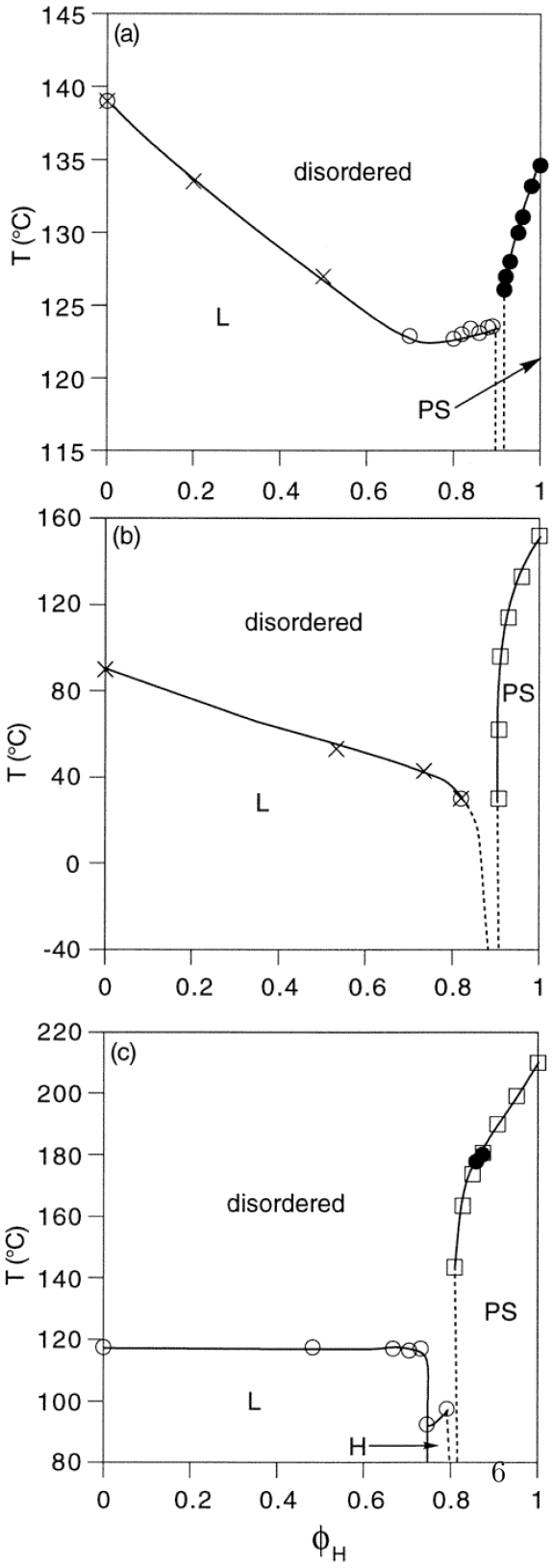

Figure 6: Phase diagrams *vs.* homopolymer volume fraction (ϕ_H) and temperature for three different block copolymer/homopolymer systems from Ref. [Hillmyer et al.(1999)Hillmyer, Maurer, Lodge, Bates, and Almdal], (a) PE-

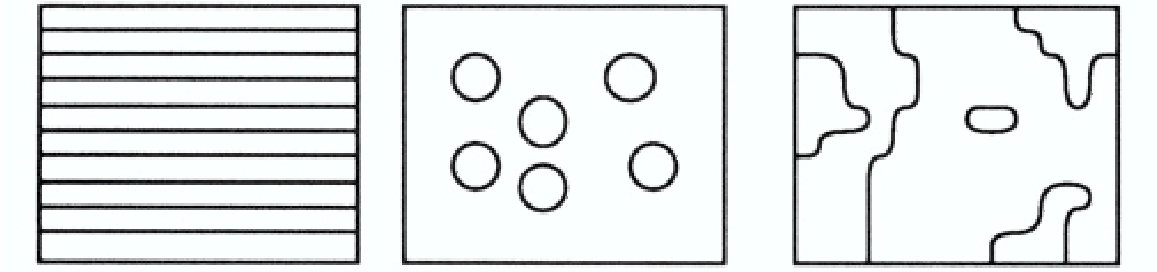

Figure 7: Schematic two-dimensional cuts through different three-dimensional membrane arrangements: Left: Lamellar phase, in which the membranes are packed in a one-dimensionally ordered phase. Middle: Vesicle phase, in which the membranes form spherical vesicles, which are positionally disordered. Right: A disordered phase of randomly-connected membranes.

Morphology of membrane-based phases

Fig. 7 illustrates schematically three possible membrane morphologies, all of which can be realized experimentally either in two- or three-component systems. In the 2-component, solvent-ampliphile case, the membranes in question are symmetric bilayers, the vesicle phase corresponds to an L_4 phase, and the randomly-connected phase is a sponge or L_3 phase. In the 3-component, solvent-amphiphile-solvent case, the membranes are monolayers, vesicle phase is a microemulsion, while the randomly-connected phase is a bicontinuous microemulsion.

Actual images of each of these phases can be captured via cryo-transmission electron microscopy (CTEM) in a block copolymer realization, namely blends of poly(styrene-ethylene/butylene-styrene) triblock copolymer (PSEBS), which acts as a bilayer-forming amphiphile and polystyrene homopolymer (PS), which acts as the solvent.

In this presentation, we will focus on the scattering from the vesicle and bicontinuous phases. For scattering experiments on lamellar phases, the static scattering is covered in a classic paper by Cyrus Safinya and co-workers [Safinya et al.(1986)Safinya, Roux, Smith, Sinha, Dimon, Clark, and Bellocq], and the dynamics in Ref. [Sikharulidze et al.(2002)Sikharulidze, Dolbnya, Fera, Madsen, Ostrovski for example.

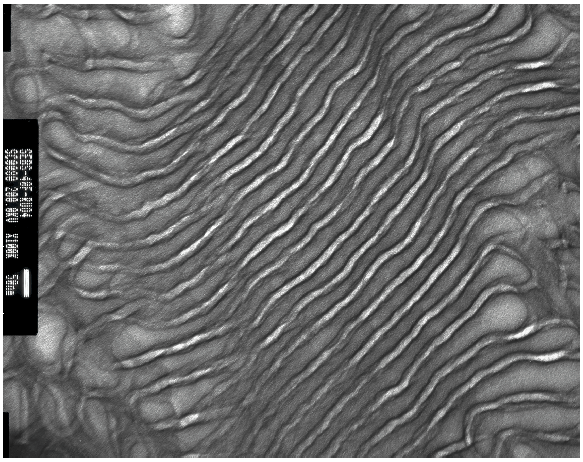

Figure 8: Lamellar phase in PSEBS-in-PS, realized for PSEBS volume fractions greater than about 0.35

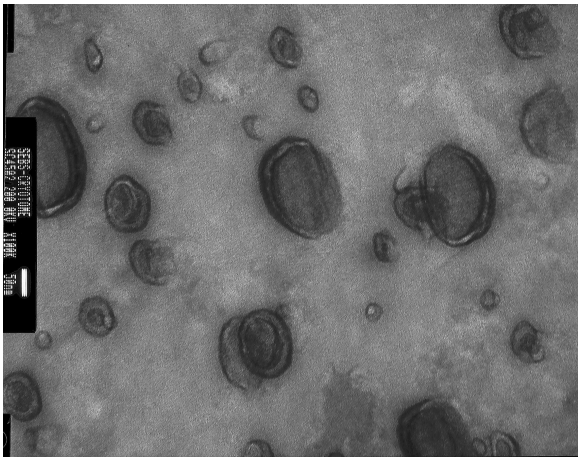

Figure 9: PSEBS-in-PS vesicles, realized for PSEBS volume fractions less than about 0.20

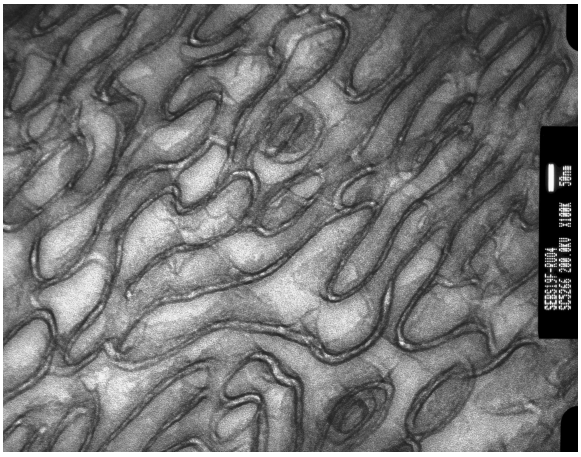

Figure 10: PSEBS-in-PS sponge, realized for PSEBS volume fractions greater than about 0.20 and less than about 0.35.

Membrane free energy

There have been a number of different approaches to understanding the phase behavior of amphiphilic systems, including

- Lattice models.
- Landau-Ginsberg-type models. I will introduce one later.
- Membrane models:

$$F = \int dA \left[\frac{\kappa}{2}(c_1 + c_2 - 2c_0)^2 + \bar{\kappa} c_1 c_2 \right], \tag{1}$$

where c_1 and c_2 are the curvatures in two perpendicular directions, c_0 is the spontaneous curvature, κ is the bending rigidity, and $\bar{\kappa}$ is the saddle-splay modulus [Helfrich(1973)]. For a symmetric, bilayer membrane $c_0 = 0$, *i.e.*

$$F = \int dA \left[\frac{\kappa}{2}(c_1 + c_2)^2 + \bar{\kappa} c_1 c_2 \right]. \tag{2}$$

which can be re-written

$$F = \int dA \left[\frac{\kappa + \bar{\kappa}/2}{2}(c_1 + c_2)^2 + \frac{-\bar{\kappa}}{2}(c_1 - c_2)^2 \right], \tag{3}$$

which is an especially convenient form for discussing the stability of a flat bilayer with respect to the formation of vesicles (which will occur when $\kappa + \bar{\kappa}/2 < 0$) or saddles (which will occur when $\bar{\kappa} > 0$). This is discussed in more detail in two independent, seminal papers [Morse(1994), Golubovic(1994)].

Droplet oil-water-surfactant microemulsions

The first specific example we consider is the example of elegant neutron scattering experiments [Huang et al.(1987)Huang, Milner, Farago, and Richter, Farago et al.(1990)Farago, Richter, Huang, Safran, and Milner] on droplet microemulsions, in which more-or-less dilute, more-or-less spherical droplets of oil (decane) are thermodynamically stable in water, by virtue of a surfactant (AOT) monolayer membrane that surrounds each one. The droplet radius is about 5 nm.

In this experiment, both deterated water and deuterated decane were employed, both of which are more-or-less readily available, whereas the AOT was ordinary, hydrogenated AOT. Consequently, the scattering length density of the oil and water regions turns out to be very similar, but quite different from that of the AOT. Thus, this is an example of an experiment carried out in *film contrast*, in which the scattering experiment is really looking only at (the behavior of) the amphiphilic film.

In this case, too, the droplets are dilute enough that it is not necessary to consider correlations between different droplets, and we need only consider the scattering from isolated droplets. An important wrinkle is that the droplets' shapes necessarily undergo thermal fluctuations – i.e. the droplets wobble. To account for this we take the density of a droplet to be that of a shell, whose radius is a function of spherical polar coordinates [θ and ϕ] and time (t):

$$R(\theta, \phi, t) = R_0[1 + \Sigma_{l,m(l\neq 1)} a_{l,m}(t) Y_{l,m}(\theta, \phi)], \tag{4}$$

where R_0 is the mean radius, and the fluctuation amplitudes, $a_{l,m}$, are determined from the membrane free energy (Eq. 2) by equipartition to be

$$< |a_{l,m}|^2 >= \frac{k_B T}{4\kappa \left(3 - 2l(l+1) + [(l+1)l/2]^2 - (A/2)[1 - l(l+1)/2]\right)}, \tag{5}$$

with $A = 4R_0/R_S - 3\bar{\kappa}/\kappa$, where $R_S = 2/c_0$ is the spontaneous radius of

curvature of the membrane [Milner and Safran(1987)]. (c_0 is the spontaneous curvature.)

Note that $l = 0$ corresponds to polydispersity, which we treated in the first lecture.

Also, note that $l = 1$ corresponds to a translation of the droplet, which does not alter the droplet shape or size.

Milner and Safran also showed that

$$< a_{l,m}(t)a_{l,m}(0) >=< |a_{l,m}|^2 > e^{-\Gamma_{l,m}t} \tag{6}$$

with

$$\Gamma_{l,m} = \frac{\kappa}{\eta R_0^3}\left[\frac{[(l+3)(l-2)+A]l(l+1)(l+2)(l-1)}{(2l+1)(2l^2+2l-1)}\right] \tag{7}$$

It follows that the scattering length density of a droplet is

$$b(\mathbf{r},t) = \Delta b_{2D}\delta(|\mathbf{r}-\mathbf{r}_V| - R(\theta,\phi,t)), \tag{8}$$

where Δb_{2D} is the excess scattering length per unit area of the membrane, and $\mathbf{r}_V$ is the coordinate of the droplet's center, which in $\mathbf{Q}$-space reads:

$$b(\mathbf{Q},t) = e^{i\mathbf{Q}\cdot\mathbf{r}_V}\frac{\sin(QR)}{QR}. \tag{9}$$

Thus, using the general relationship between the $b(\mathbf{Q},t) = \Sigma_i b_i e^{i\mathbf{Q}\cdot\mathbf{r}_i}$ and the ISF, it is straightforward to show – using that $\mathbf{r}_V$ and the collection of all the $a_{l,m}$ are independent, random variables – that

$$S(Q,t) = e^{-DQ^2t}(\Delta b_{2D})^2\left[< p_0(QR_0) > +\Sigma_{l>1}\frac{2l+1}{4\pi} < p_l(QR_0) >< |a_{l,0}|^2 > e^{-\Gamma_{l,0}t},\right] \tag{10}$$

where

$$p_0(x) = [j_0(x)]^2 + j_0(x)\Sigma_{l>1}\frac{2l+1}{4\pi} < |a_{l,0}|^2 > \left[[2-x^2+l(l+1)]j_0(x) - 2xj_1(x)\right], \tag{11}$$

$$p_l(x) = [(l+2)j_l(x) - xj_{l+1}(x)]^2, \tag{12}$$

j_n is the spherical Bessel function of order n [Huang et al.(1987)Huang, Milner, Farago, and Richter Farago et al.(1990)Farago, Richter, Huang, Safran, and Milner], and the $<$ .... $>$ about $p_l(x)$ denote an average over the polydispersity, given by $<$

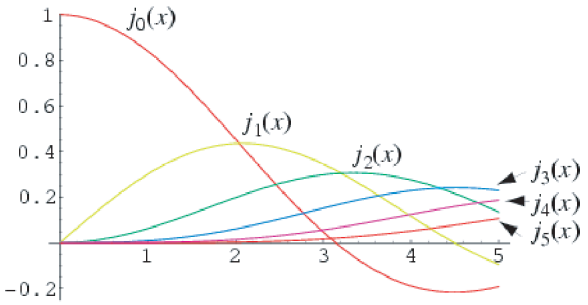

Figure 11: Spherical Bessel functions, $j_n(x)$ versus x, for $n = 0$ through 5.

$|a_{0,0}|^2 >= K_BT/[4\kappa(6-A)]$. To derive Eq. 10, we also used that $< a_{l,m}a_{l',m'} >= \delta_{l,l'}\delta_{m,m'} < |a_{l,0}|^2 >$.

Plotted in Fig. 11 are the first few spherical Bessel functions. Interestingly, $j_0(\pi) = 0$, but $j_2(\pi) \neq 0$. Therefore, at $QR = \pi$, we may expect NSE measurements to be especially sensitive to the $l > 1$ modes, *i.e.* to the droplet wobble.

The zero time limit of Eq. 10 is the static structure factor. Examples from Ref. [Farago et al.(1990)Farago, Richter, Huang, Safran, and Milner] are shown in Fig. 12. The different curves correspond to different amount of a cosurfactant, butanol, which changes κ and hence the polydispersity, tending to fill in the minimum near $QR_0 = \pi$.

Fig. 13 shows the pertinant NSE data from Ref. [Huang et al.(1987)Huang, Milner, Farago, and These data are plotted on a logarithmic scale for $S(Q,t)/S(Q)$ and a linear t scale, so that simple, single exponentials appear as straight lines. Looking at the data, it is clear that the data are consistent with a simple exponential over the range of times probed, which is short times as far as the ISF is concerned. Indeed, the solid lines correspond to a single exponential form for the ISF within the time range studied. The corresponding relaxation rate, we identify with the short-time relaxation rate ($\Gamma_S = D_{eff}Q^2$, where D_{eff} is the short-time diffusion coefficient).

How then do these data mesh (or not) with Eq. 10? To make a comparison, we may expand $S(Q,t)/S(Q)$ to linear order in t. Specifically, assuming that only the $l = 2$ mode gives a significant contribution to $S(Q)$ – note that $< |a_{l,0}|^2 >$ does decrease with increasing l – we find that

$$S(Q,t)/S(Q) \simeq 1 - D_{eff}Q^2t. \tag{13}$$

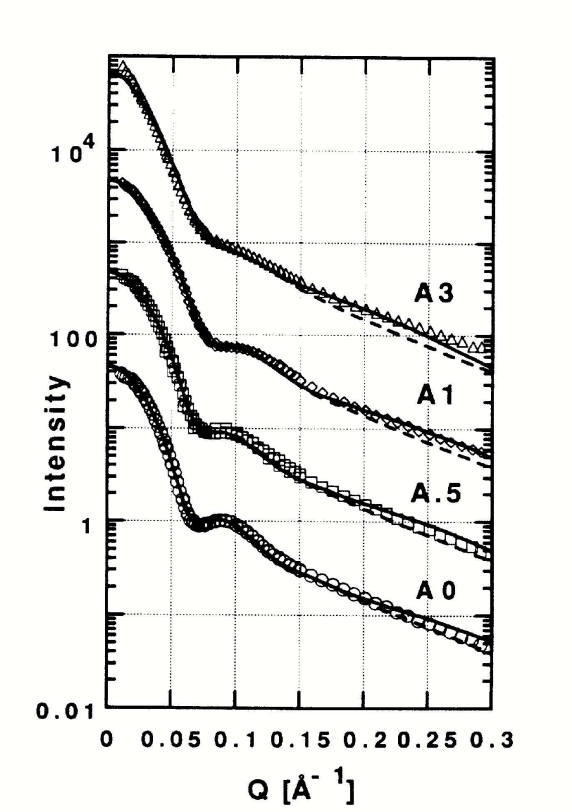

Figure 12: SANS profiles for AOT-water-decane microemulsions with added butanol cosurfactant. The concentration of butanol increases from A0 to A3.

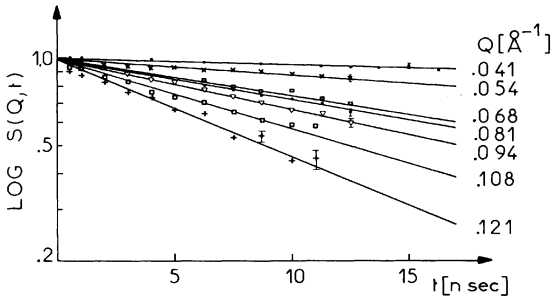

Figure 13: $S(Q,t)$ versus t for a droplet microemulsion. The solid lines are fits to a single exponential form.

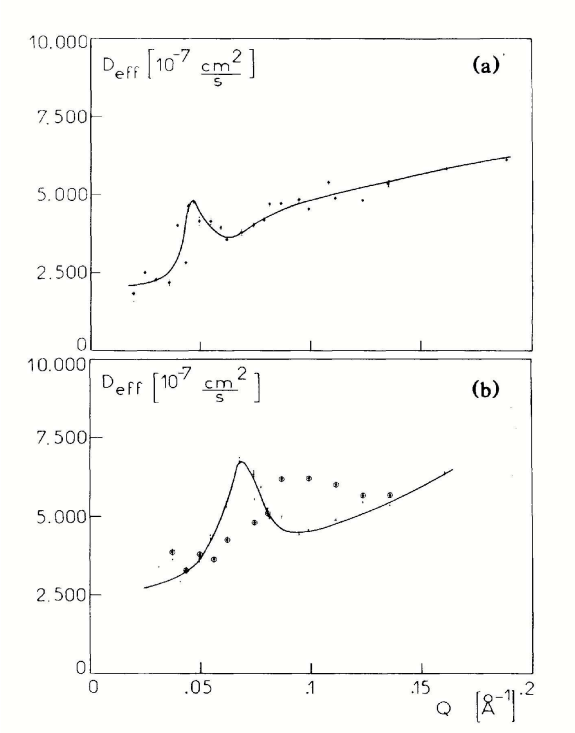

Figure 14: Short time diffusion coefficient (D_{eff}) vs. Q for an AOT-water-oil droplet microemulsion.

with

$$D_{eff} = \frac{D < p_0(QR_0) > +(D + \Gamma_{2,0}/Q^2)(5 < |a_{2,0}|^2 > /4\pi) < p_2(QR_0) >}{< p_0(QR_0) > +(5 < |a_{2,0}|^2 > /4\pi) < p_2(QR_0) >}. \tag{14}$$

We expect that D_{eff} shows a peak near $QR_0 = \pi$, since $< p_0(\pi) >$ is small.

In comparison, Fig. 14 shows the measured values of D_{eff} from Ref. [Huang et al.(1987)Huang, Milner, Farago, and Richter], and indeed D_{eff} shows a peak near $QR_0 \simeq \pi$ consistent with theory.

Sponge phases

As we move to now consider the sponge phase and its scattering, we can no longer focus attention on isolated spheres. So what can we do?

Last time, we discussed that $S(Q)$ was related to the correlation function

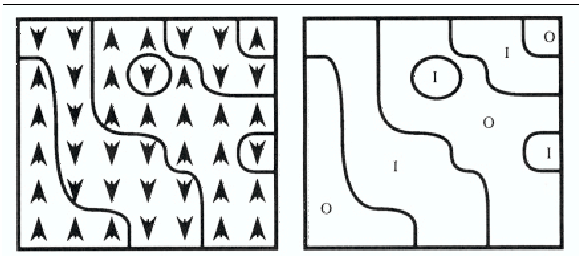

Figure 15: Lines representing bilayer membranes in a sponge phase. Right: Since the membranes (lines) are assumed not to end, nor to form junctions, each volume of solvent lies inside (I) or outside (O) the membrane. Thus, we may introduce an order parameter – the I/O order parameter – that specifies whether a given point is inside or outside the membrane. Left: The I/O order parameter is equivalent to the order parameter of an Ising spin model, with O corresponding to spin up and I to spin down.

of whatever was giving rise to the scattering – inhomogeneities in the electron density (x-ray), in the scattering length density (neutrons), or in the refractive index density (light).

So if we can write down a free energy and thus calculate a correlation function, why then it should be possible to calculate $S(Q)$. This is the program for the sponge phase.

Cates et al. [Cates et al.(1988)Cates, Roux, Andelman, Milner, and Safran, Roux et al.(1992)Roux, Coulon, and Cates] noticed that if membranes are assumed not to have edges, nor to form T-junctions, because these defects cost too much free energy, why then it is possible to introduce an Ising-type order parameter (Φ) that specifies whether a given point is inside or outside the membrane. There may be I/O symmetry, which would correspond to the disordered phase of the Ising model, or there may be more solvent outside than inside which would correspond to the ordered phase of the Ising model.

It is important to emphasize that in sponge phases the I and O regions are actually the same material – both water for example. Therefore, there is no scattering associated with Φ fluctuations.

In addition, to the I/O order parameter, a Landau-Ginzberg-type description of the sponge phase should also account for the amphiphile density via another order parameter (ρ), which is proportional to the difference in amphiphile density from some reference density. (Since, in general, there is

scattering constrast associated with the amphiphile density, scattering experiments will measure the ρ correlations.) Incorporating the $\Phi - \rho$ coupling in the simplest-possible fashion [Roux et al.(1992)Roux, Coulon, and Cates], we arrive at a candidate, in-fact-over-simplified, free energy density, but which (it turns out) can be solved for what we need:

$$F(\Phi, \rho) = g_0(\nabla\Phi)^2 + \omega_2\Phi^2 + \omega_4\Phi^4 + \beta\rho^2 + \gamma_1\rho\Phi^2, \tag{15}$$

which is equivalent to the Blume-Emergy-Griffiths model [Blume et al.(1971)Blume, Emery, and Gr which, in turn, describes the behavior of He3-He4 mixtures!! In any case, minimizing Eq. 15 allows for a symmetric phase ($< \Phi >= 0$) and an asymmetric phase ($< \Phi > \neq 0$), and either a countinuous (second order) or discontinuous (first order) phase transition between them, as the parameters of Eq. 15 are varied.

Note that Eq. 15 gives rise to a Gaussian probability distribution for ρ with mean $-\Phi^2(r)/(4\beta)$. (Exercise: prove this.) It follows that:

- We can integrate over $\rho(r)$ exactly, so that

$$F(\Phi) = g_0(\nabla\Phi)^2 + \omega_2\Phi^2 + \omega_4(1 - \gamma_1^2\omega_2)\Phi^4 \tag{16}$$

- The surfactant density-density correlation function is [Roux et al.(1992)Roux, Coulon, and Ca

$$< \rho(r)\rho(r) >= g(r) = \frac{\gamma_1^2}{16\beta}[< \Phi^2(r)\Phi^2(0 > - < \Phi^2 >^2] + \frac{1}{2\beta}\delta(r) = \frac{\gamma_1^2}{8\beta} < \Phi(r)\Phi(r) >^2 + \frac{1}{2\beta}\delta(\tag{17}$$

  where the last step further assumed that $\Phi(r)$ is a Gaussian random variable (GRV) (which should be OK far from any second-order phase transition).

For small enough $\omega_4(1 - \gamma_1\omega_2)$, $\Phi(r)$ is a GRV and it may be shown that

$$< \Phi(r)\Phi(0) >= \frac{e^{r/\xi}}{8\pi g_0 r}, \tag{18}$$

with $\xi = \sqrt{g_0/\omega_2}$. This is the so-called Ornstein-Zernicke form for the correlation function, and gives rise to a correlation function in Q-space:

$$S_{\Phi\Phi}(Q) = \frac{1}{2\omega_2(1 + (\xi Q)^2)}, \tag{19}$$

but, of course, there is no scattering constrast associated with $S_{\Phi\Phi}$.

From Eq. 17 and Eq. 18, we deduce that

$$g(r) = \frac{\gamma_1^2}{16\omega_2}\frac{e^{-2r/\xi}}{(8\pi g_0 r)^2} + \frac{1}{2\omega_2}\delta(r), \tag{20}$$

whose Fourier transform is

$$S_{\rho\rho}(Q) = C_1\left[C_2 + \frac{\gamma_1^2 \arctan(q\xi/2)}{Q\xi/2}\right], \tag{21}$$

with $C_1 = \xi/(256\pi\omega_2^2 g_o^2)$ and $C_2 = 128\pi\omega_2 g_0^2/\xi$, and which does give rise to scattering. The first term corresponds to the ρ scattering without coupling to Φ. The second term is the effect of the $\rho - \Phi$ coupling.

The Q-dependence predicted by Eq. 21 for $Q\xi > 1$ is that $S_{\rho\rho}(Q) \simeq 1/Q$. By constrast, in the more usual case, such as for $S_{\Phi\Phi}$ in Eq. 19, for $Qxi > 1$, $S_{\Phi\Phi}(Q) \simeq 1/Q^2$. Therefore, the sponge phase has an unusual signature in its scattering.

0.0.1 Comparison to experiment

Is this unusual form realized? Fig. 16 from Ref. [Roux et al.(1990)Roux, Cates, Olsson, Ball, Nallet plots measurements of $[S_{\rho\rho}(Q)]^{-1}$ versus Q obtained via static light scattering from a sponge phase in dodecane-SDS mixtures with a pentanol cosurfactant, which (presumably) has the role of tuning the properties (*i.e.* κ and $ka\bar{p}pa$) of the sponge's constituent bilayer.

Fig. 17 shows how ξ and $S(0)$, determined by fits to a form similar to Eq. 21, vary as a function of cosurfactant (pentanol) volume fraction. Evidently, both quantities tend to diverge near a volume fraction of 0.02. This is just the behavior expected near a continuous, second order phase transition. What is especially remarkable in this case is that the correlation length in question is not the correlation length of the ρ fluctuations, but of the Φ fluctuations.

0.0.2 Many sponge phases show a peak!

Fig. 18 shows a CCD image of the SAXS pattern from the PSEBS-in-PS sponge shown in Fig. 19, *i.e.* Notice that, in addition to a peak in the scattering at $Q = 0$, there is also a clear ring of scattering at non-zero Q. This peak lies outside of the theoretical description presented so far. In fact, as shown in Fig. 20 [Falus et al.(2004)Falus, Xiang, Borthwick, Russell, and Mochrie],

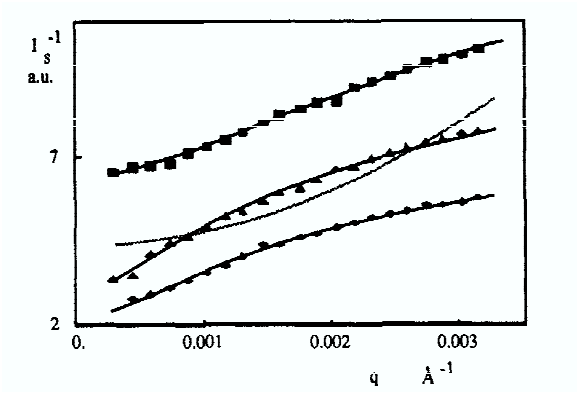

Figure 16: Inverse scattering intensity versus Q for a decane-SDS-pentanol sponge at three different concentrations. Data are the solid points. Lines through the data are fits to a model for the sponge phase scattering $S_{\rho\rho}(Q)$, similar to Eq. 21. The other line is a best fit to the Ornstein-Zernike form for $S\rho\rho(Q)$ and evidently does not describe the data.

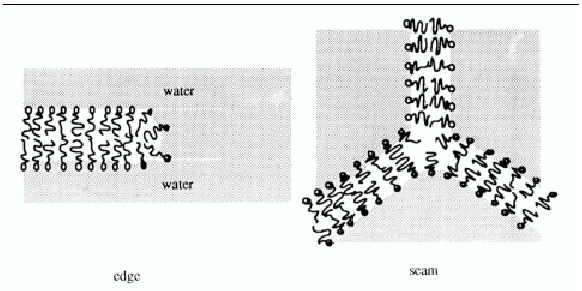

Figure 17: Correlation length, ξ, and zero-Q inverse scattering intensity, $S^{-1}(Q)$, plotted versus pentanol volume fraction (ϕ) for the pseudo-binary system of water and SDS-pentanol

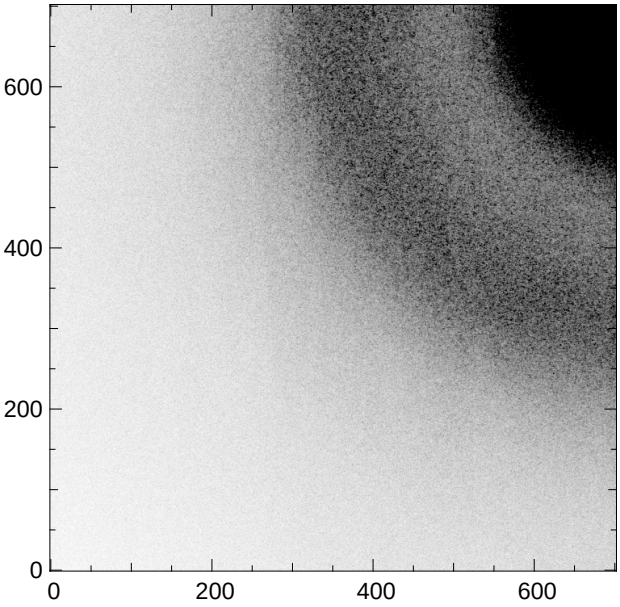

Figure 18: Grey-scale representation of a 700×700 pixel region showing the PSEBS-PS L_3-phase SAXS obtained at beamline 8-ID at the Advanced Photon Source.

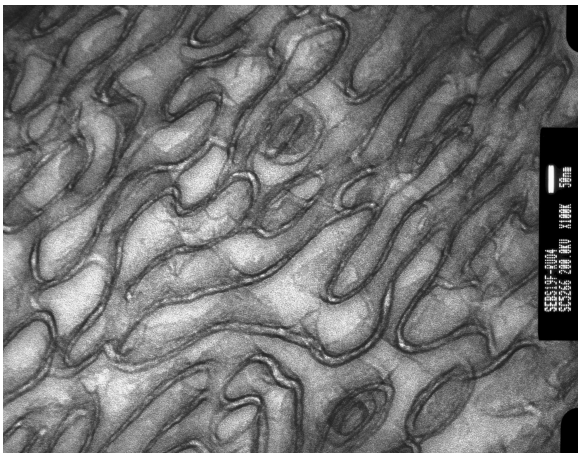

Figure 19: PSEBS-in-PS sponge, realized for PSEBS volume fractions greater than about 0.20 and less than about 0.4.

the PSEBS-in-PS sponge-phase peak position varies linearly with surfactant volume fraction, as is the case in many other systems.

0.0.3 Neutron scattering from bicontinuous microemulsions

Sponge phases occur in 2 component bilayer systems, and the bilayer membrane separates the water (say) volume into 2 distinct parts: I and O. On the other hand, it is easy to envision simultaneously replacing either I or O by oil and the bilayer by a monolayer. The result is a *bicontinuous microemulsion* (BμE).

To understand the peak in the scattering from sponge phases, neutron scattering experiments from BμE phases using contrast variation have been very instructive. Fig. 21 shows two SANS profiles. The top curve is SANS from a sponge phase and the scattering can derive solely from the film. The lower curve is SANS from a BμE *studied in film contrast*, so that the oil and water have essentially identical scattering length densities, which is very different from the scattering length density of the monolayer that separates the oil and water. Thus, in this case too the experiment is looking at the membrane only. Clearly, the profiles are very similar. This is not a surprise, since we already said that these two phases were analogues of each other.

But now possessing this information, it is possible to now examine the BμE under *bulk contrast*, which should allow us to examine our assumptions about the Φ correlations, since for neutron scattering in bulk contrast, with e.g. D_2O and $C_{10}H_22$, $S_{\Phi\Phi}$ is actually measureable.

Fig. 22 shows two SANS profiles from the same BμE, one obtained under film contrast, which looks like what we are now used to, and the other obtained under film contrast, whihc shows a sharp peak at a smaller Q than in film constrast – quite different from what we assumed in our earlier discussion. Why are the peaks under film and bulk contrast at different positions? For film contrast, the peak corresponds to the mean film-to-film distance, while for bulk contrast, the peak corresponds to the mean water-to-water repeat distance, which is roughly twice the film-to-film distance because the water regions are spaced by oil regions.

Fig. 22 suggests that origin of the usual peak at non-zero Q in the scattering from many realizations of the sponge phase comes from a peak in $S_{\Phi\Phi}$. This idea was quantified by Gompper and Schick [Gompper and Schick(1994)] who used a modified form (Teubner-Strey form) for $S_{\Phi\Phi}$ and added to the

Landau-Ginsberg free energy all the terms allowed by symmetry:

$$F(\Phi,\rho) = F_0(\Phi) + F_1(\rho) + F_2(\Phi,\rho), \tag{22}$$

where

$$F_0(\Phi) = \int d^3r \left[c\left(\nabla^2\Phi^2\right) + g_0\left(\nabla\Phi\right)^2 + \omega_2\Phi^2\right], \tag{23}$$

$$F_1(\rho) = \int d^3r \left[\alpha\left(\nabla\rho\right)^2 + \beta\rho^2\right], \tag{24}$$

and

$$F_2(\Phi,\rho) = \int d^3r \left[\gamma_1\rho\Phi^2 + \gamma_2\left(\nabla^2\rho\right)\Phi^2 + \gamma_3\rho\Phi\left(\nabla^2\Phi\right)\right]. \tag{25}$$

Implicit in this expression is that

$$S^0_{\Phi\Phi} = \frac{1}{2c[(Q^2 - k^2 + \xi^{-2})^2 + 4k^2\xi^{-2})]}, \tag{26}$$

where

$$k^2 = \frac{1}{2}\sqrt{\frac{\omega_2}{c}} + \frac{1}{4}\frac{g_0}{c}, \tag{27}$$

and

$$\xi^{-2} = \frac{1}{2}\sqrt{\frac{\omega_2}{c}} + \frac{1}{4}\frac{g_0}{c}, \tag{28}$$

are the wavevector and (inverse) correlation length (squared) of the I/O order.

Using Eq. 25, Gompper and Schick were able to derive a modifed expression for $S_{\rho\rho}$ that agree well with experiment as shown by the solid lines in Fig. 20.

Dynamics of individual membranes

At large enough Qs, the ISF of even a collection of membranes in a vesicle or sponge phase, we expect to reflect the Brownian motion of an individual isolated membrane. The sort of dynamics we have in mind is shown in this movie, which came from an IBM Almaden web site, and which I guess was created by Farid Abraham.

Theory of the dynamics of individual membranes

The dynamics of membranes has been discussed by Frey and Nelson [Frey and Nelson(1991)] and Zilman and Granek [Zilman and Granek(1996), Zilman and Granek(2002)].
As we saw in Sam Safran's lectures, membrane undulations are naturally specified by giving the membrane's height (h) above some arbitrary plane whose normal is parallel to the membrane's mean surface normal. We also saw that these undulations are controlled by an effective Hamiltonian

$$H = \frac{1}{2}\kappa \int d^2r [\nabla^2 h(r)]^2 = \frac{1}{2}\kappa \Sigma_k k^4 h_k h_{-k} \tag{29}$$

It can be shown that this leads to a relaxation rate for a mode of wavenumber k of

$$\Gamma_k = \frac{1}{4\eta k}\kappa k^4 = \frac{\kappa k^3}{4\eta} \tag{30}$$

i.e. the product of a kinetic coefficient (here the Oseen interaction in k-space) and an inverse suspectibility to height fluctuations.

It follows that

$$< h_k(t) h_{-k}(0) >= \frac{k_B T}{\kappa k^4} e^{-\Gamma_k t} \tag{31}$$

and, after some algebra,

$$< [h(r,t) - h(r',0)]^2 > \simeq \frac{k_B T}{4\pi\kappa}(r-r')^2 \log(\xi/|r-r'|) + \left[0.069 (\frac{k_B T}{\kappa})^{1/2} \frac{k_B T}{\eta} t\right]^{2/3}. \tag{32}$$

For a thin membrane, the excess density is a δ-function located at the membrane, *i.e.* $b(\mathbf{x}, t) = (\Delta b)\delta(z - h(\mathbf{r}))$. (Here $\mathbf{x}$ is a 3D position vector, while $\mathbf{r}$ is a 2D position vector, and Δb is the scattering length per unit area of the membrane.) Whence we may deduce that the ISF is related to the mean square height difference via

$$S(Q,t) = \int d^2r \int d^2r' e^{iQ_{||}\cdot(r-r')} e^{-Q_z^2 < [h(r,t) - h(r',0)]^2 >} \simeq S(Q) e^{-[0.025 (k_B T)^{3/2} Q_z^3 t/(\kappa^{1/2}\eta)]^{2/3}}. \tag{33}$$

This is for a membrane with surface normal along z. Averaging over orientations, as is appropriate for vesicle and sponge phases, gives

$$S(Q,t) \simeq S(Q) e^{-(\Gamma_Q t)^\beta}, \tag{34}$$

with

$$\Gamma_Q = 0.025 k_B T (k_B T/\kappa)^{1/2} Q^3 \eta \tag{35}$$

and

$$\beta = (2/3)[1 + (k_B T)/(4\pi\kappa)]. \tag{36}$$

0.1 X-ray PCS studies of the ISF of polymer membranes

Fig. 23 plots representative x-ray multispeckle PCS intensity autocorrelation functions obtained at 140°C for the dilute vesicle phase that occurs in PSEBS-in-PS blends [Falus et al.(2005)Falus, Borthwick, and Mochrie]. Data at four different wavevectors are plotted versus delay time on a logarithmic scale to display the entire range of times studied. Notice that the signal-to-noise ratio (SNR) gets increasing poorer as Q increases. This is because the scattering strength decreases with Q. Nevertheless, these data are of high enough quality to make feasible investigations of the autocorrelation line shapes.

Inspired by the Zilman-Granek predictions, we fit the g_2s to the form expected for a stretched-exponential ISF (Eq. 34). The resultant best-fit model g_2s, which are shown as the solid lines in Fig. 23, provide an excellent description of the experimental data. To clarify the extent to which these data require a stretched exponential ISF rather than a strictly exponential form, in Fig. 24, we present ISFs $[f(q,t) = \sqrt{(g_2 - 1)/A}]$ obtained at 160°C, plotted as the open symbols versus reduced delay time, Γt, where t is the delay time and Γ is the best fit relaxation rate for the data in question. The solid lines in Fig. 24 are the ISFs corresponding to the best-fit model g_2s. The logarithmic intensity scale and linear time scale of this figure imply that an exponential ISF (*i.e.* $\alpha = 1$) would appear as a straight line. By contrast, the measured ISFs clearly exhibit a small curvature, demonstrating a deviation from single-exponential relaxation.

Stretched exponential fits were carried out for data obtained at each temperature studied, and for each wavenumber partition. The best-fit stretching exponents are shown in Fig. 25 for 180°C (circles), 160°C (triangles), and 140°C (squares). Evidently, the stretching exponent is only weakly-dependent on wavevector and temperature with a value of about $\alpha \simeq 0.8 \pm 0.1$. A stretched-exponential ISF with a stretching exponent that is slightly larger than $\alpha = 2/3$ is consistent with the prediction of Ref. [Zilman and Granek(2002)]

(Eq. 34), where a stretching exponent in the range between 0.7 and 0.9 would correspond to a value for κ between 1.7 and $0.23k_BT$.

The corresponding best-fit relaxation rates increase rapidly and monotonically with increasing wavevector (q) in a more-or-less power-law fashion, with similar exponents at each temperature. In addition, they show a strong temperature dependence, with significantly faster relaxations at higher temperatures. Because the PS homopolymer viscosity decreases by a factor of about forty as the temperature is increased from 140°C ($\eta \simeq 240$ Poise) to 180°C ($\eta \simeq 6$ Poise) [Fox and Flory(1950), Plazek and O'Rourke(1971)], according to Eq. 35, we should expect the temperature dependence of the relaxation rate to be dominated by the PS viscosity. For $\kappa \simeq k_BT$, ν is small, and it is sensible to approximate $\nu \simeq 0$. In this case, the relaxation rate (Γ) is predicted to vary nearly linearly versus k_BTq^3/η. Thus, according to the Zilman-Granek-Nelson-Frey model we expect the *reduced relaxation rate*, $\Gamma\eta/(k_BTQ^3)$ to be independent of Q and temperature.

NSE measurements of the membrane dynamics of bicontinuous microemulsions

Similar behavior has also been observed in other membrane-based phases, including in highly swollen L_α and L_3 phases, which were studied via dynamic light scattering [Freyssingeas et al.(1997)Freyssingeas, Roux, and Nallet], and in bicontinuous microemulsion phases, which were studied using the NSE technique under film contrast conditions [Mihailescu et al.(2001)Mihailescu, Monkenbusch, Endo, A
This is illustrated in the latter case in Fig. 27, which shows the ISF of a water-decane-$C_{10}E_4$ microemulsion at several values of Q.

Notice that at the longest times accessible (160 ns), at the smallest Q shown (0.3 nm^{-1}, the ISF has fallen to only about 0.8 of its original value.

0.1.1 Dynamics of a polymer sponge phase

Several studies have addressed the dynamical behavior of the L_3 phase [Milner et al.(1990)Milner, C
Porte et al.(1991)Porte, Delsanti, Billard, Skouri, Appell, Marignan, and Debeauvais,
Granek and Cates(1992), Waton and Porte(1993), Gompper and Hennes(1994),
Hennes and Gompper(1996), Freyssingeas et al.(1996)Freyssingeas, Nallet, and Roux,
Nonomura and Ohta(1999), Schwarz et al.(2000)Schwarz, Monch, Ilgenfritz, and Strey,
Mihailescu et al.(2001)Mihailescu, Monkenbusch, Endo, Allgaier, Gompper, Stellbrink, Richter, Ja
Komura et al.(2001)Komura, Takeda, Kawabata, Ghosh, Seto, and Nagao, Holderer et al.(2005)H

However, except in a few special cases [Freyssingeas et al.(1996)Freyssingeas, Nallet, and Roux, Mihailescu et al.(2001)Mihailescu, Monkenbusch, Endo, Allgaier, Gompper, Stellbrink, Richter, Ja it has so-far proven difficult to experimentally examine the relaxation of equilibrium fluctuations at wavevectors (Q) most characteristic of the L_3 phase, near the peak of the static scattering. On the theoretical side, Milner *et al.* [Milner et al.(1990)Milner, Cates, and Roux] have given a physically appealling formulation that postulates three slow modes: one associated with Φ, another associated with ρ, and the third corresponding to topological relaxation, via the creation and dissolution of membrane necks. The latter processes are activated. Therefore, topological relaxation may be expected to be especially slow. Alternatively, Gompper and Hennes [Gompper and Hennes(1994), Hennes and Gompper(1996)] have presented field-theoretic calculations that incorporate the coupling between ρ and Φ required to explain the observed L_3-phase static scattering. They also incorporate couplings of ρ and of Φ to the transverse momentum density, which they include as an additional slow variable. In this treatment, the membrane topology does not appear explicitly.

A selection of normalized ISFs, for the PSEBS-in-PS sponge phase ($\phi = 0.20$) obtained at 180°C, are plotted in Fig. 29 on a logarithmic scale versus reduced delay time on a linear scale. The logarithmic intensity and linear time scale of this figure implies that simple exponentials would appear as straight lines. Evidently, the measured ISFs at 180°C exhibit a clear deviation from straight lines, indicating that the ISFs in this case do not show simple exponential relaxations. Indeed, the positive curvature of these data imply stretched-exponential or double-exponential behavior of the ISF. The data were fitted using both a stretched/compressed exponential form for the ISF, $f(Q,t) = \exp[-(\Gamma t)^{\beta}]$ with Γ and β as fitting parameters, and a double exponential form for the ISF, $f(Q,t) = a_F \exp(-\Gamma_F t) + a_S \exp(-\Gamma_S t)$, with $a_S = 1 - a_F$, Γ_F, and Γ_S ($\Gamma_F > \Gamma_S$) as fitting parameters. Both forms yield a good description of the data, but to better try to make contact with theory, we focussed on the double exponential description, and the solid lines in the figure show the double exponential fits. Reduced time in this case is $\Gamma_I t$, where $\Gamma_I = a_F\Gamma_F + a_S\Gamma_S$ is the initial decay rate.

In striking contrast to the data at 180°C, at 120°C the ISFs, plotted on logarithmic intensity and linear time axes in Fig. 30, clearly show negative curvature. Thus, instead of a stretched exponential, at 120°C, the ISF exhibits a *compressed* exponential form (solid lines).

Now, recently, it has been proposed [Liu and Nagel(1998)] that a wide

range of highly-structured but disordered soft matter – including, gels [Cipelletti et al.(2000)Cipellet
foams [O'Hern et al.(2001)O'Hern, Langer, Liu, and Nagel], clays [Bandyopadhyay et al.(2004)Ban
suspensions [Trappe et al.(2001)Trappe, Prassad, Cipelletti, Segre, and Weitz,
Pham et al.(2002)Pham, Puertas, Bergenholtz, Egelhaaf, Moussaid, Pusey, Schofield, Cates, Fuchs
Bellour et al.(2003)Bellour, Knaebel, Harden, Lequeux, and Munch], and emulsions [Cipelletti et al.(2003)Cipelletti, Ramos, Manley, Pitard, Weitz, Pashkovski, and Johansson] – can exhibit a *jamming* transition from a fluid to a solid-like state with arrested dynamics.

Moreover, a variety of materials in a putative jammed state display *compressed* exponential ISFs [Cipelletti et al.(2000)Cipelletti, Manley, Ball, and Weitz,
Cipelletti et al.(2003)Cipelletti, Ramos, Manley, Pitard, Weitz, Pashkovski, and Johansson,
Bandyopadhyay et al.(2004)Bandyopadhyay, Liang, Yardimci, Sessoms, Borthwick, Mochrie, Hard suggesting that such ISFs may be a key signature of the jammed state. Such a form for the ISF has been explained on the basis of the relaxation of force dipoles randomly distributed throughout the sample [Cipelletti et al.(2000)Cipelletti, Manley, Ball, Bouchard and Pitard(2001), Cipelletti et al.(2003)Cipelletti, Ramos, Manley, Pitard, Weitz, Pashk This picture also predicts a linear variation of the characteristic relaxation rate with Q. The jammed state often undergoes aging, which is manifest as an decrease in the the characteristic relaxation rate with aging time [Cipelletti et al.(2000)Cipelletti, Manley, Ball, and Weitz, Bellour et al.(2003)Bellour, Knaebel, Ha
Cipelletti et al.(2003)Cipelletti, Ramos, Manley, Pitard, Weitz, Pashkovski, and Johansson,
Bandyopadhyay et al.(2004)Bandyopadhyay, Liang, Yardimci, Sessoms, Borthwick, Mochrie, Hard In the present case, data obtained at 120°C after an aging time of 7000 s are indistinguishable from those obtained after an aging time of 15000 s (data not shown). It follows that any aging-time dependence of the relaxation rate at 120°C within this time range would have to be much weaker than those reported in Refs. [Cipelletti et al.(2000)Cipelletti, Manley, Ball, and Weitz,
Bellour et al.(2003)Bellour, Knaebel, Harden, Lequeux, and Munch, Bandyopadhyay et al.(2004)B However, aging-time-independent behavior has also been observed in Pluronic micellar polycrystals [Cipelletti et al.(2003)Cipelletti, Ramos, Manley, Pitard, Weitz, Pashkovski,

We summarize in Fig. 31 our results for the Q-dependence of the *reduced* relaxation rates, defined as $\Gamma_R = \Gamma_M/\Gamma_0$, where Γ_M is one of Γ_F, Γ_S or Γ, and $\Gamma_0 = k_B T Q^2 Q_0/\eta_{PS}$, with Q_0 the peak of the IO correlation function ($0.036\ \mathrm{nm}^{-1}$), and η_{PS} the temperature-dependent viscosity of the PS solvent [Fox and Flory(1950)], which varies from 7 Poise at 180°C to 2200 Poise at 120°C. Also shown in this figure is the reduced relaxation rate for PSEBS-in-PS vesicles from Ref. [Falus et al.(2004)Falus, Xiang, Borthwick, Russell, and Mochrie]. In that case, data from 140°C, 160°C and 180°C collapse quite well to the

theoretical curve (soild line) for isolated membrane plaquettes, for which the relaxation rate shows a Q^3-variation [Zilman and Granek(1996)]. By contrast, for the present data at 140°C, 160°C, and 180°C, although in both cases the Q-dependence appears similar at the different temperatures, neither Γ_F/Γ_0 (solid symbols) nor Γ_S/Γ_0 collapse to a single curve: Γ_F/Γ_0 increases by a factor of 1.5-2 as the temperature is decreased from 180°C to 160°C and again from 160°C to 140°C, while Γ_S/Γ_F increases by factors of about 3 for the same temperature steps. These observations suggest that, in addition to solvent flow, processes, such as solvent permeation through the membrane, that do not depend on the solvent viscosity, are relevent for both modes. Both Γ_F/Γ_0 and Γ_S/Γ_0 appear independent of Q for $Q \leq 0.03$ nm^{-1}, indicating diffusive behavior on long length scales. A notable feature of both Γ_F/Γ_0 and Γ_S/Γ_0 is a minimum, more pronounced for Γ_S/Γ_0, occurring at or close to the value of Q , at which there is a peak in the static scattering (Fig. **??**). This is an example of the general phenomenon of "de Gennes narrowing" [de Gennes(1956)], namely that relaxations near the peak of the structure factor are especially slow. (A peak in the structure factor implies that density waves with the corresponding Q are highly prevalent. That their relaxation rate is small implies that they are long lived. This is actually something that follows in colloidal systems from the f-sum rule, by substituting $S(Q)$ for $\chi_T \bar{n} k_B T$.)

Surprisingly, at larger Qs the relaxation rates do not show the Q^3-dependence expected for independent membranes [Freyssingeas et al.(1996)Freyssingeas, Nallet, and Roux, Mihailescu et al.(2001)Mihailescu, Monkenbusch, Endo, Allgaier, Gompper, Stellbrink, Richter, Ja Komura et al.(2001)Komura, Takeda, Kawabata, Ghosh, Seto, and Nagao, Holderer et al.(2005)H and found at smaller Qs in the more dilute system [Falus et al.(2004)Falus, Xiang, Borthwick, Russe

Turning now to the data obtained at 120°C, no minimum in Γ/Γ_0 is discernable. Instead, over the range of Qs studied, which includes the peak of the static scattering, there is a smooth variation of the relaxation rate with Q, which may be described as a power law with an exponent of 1.16 ± 0.05 (solid line in the figure), similar to, but slightly larger than, the linear variation observed previously in the case of compressed exponential relaxations [Cipelletti et al.(2000)Cipelletti, Manley, Ball, and Weitz, Bellour et al.(2003)Bellour, Knaebel, Ha Cipelletti et al.(2003)Cipelletti, Ramos, Manley, Pitard, Weitz, Pashkovski, and Johansson, Bandyopadhyay et al.(2004)Bandyopadhyay, Liang, Yardimci, Sessoms, Borthwick, Mochrie, Hard

The relative amplitude of the slow mode (a_S) for the double exponential fits at 140°C, 160°C and 180°C is shown versus Q in Fig. 32(a). Overall, the amplitude of the slow decay increases towards unity with decreasing temper-

ature, with the effect that the ISFs appear progressively less stretched as the temperature decreases. In addition, at each temperature, a_S shows a peak occurring at the Q of the peak of the static scattering, which we interprete as a further manifestation of de Gennes narrowing. Fig. 32(b) shows the best-fit exponent (β) versus Q, determined from the stretched/compressed-exponential fits at 120°C. Evidently, the stretching/compression exponent varies from a peak of about 1.35 at 0.07 nm^{-1} – the peak of the static scattering again – to 1.07 at the largest Qs studied (0.2 nm^{-1}). The compressed exponential relaxation found for the PSEBS-in-PS L_3 phase at 120°C [Fig. 30 and Fig. 32(b)], together with a relaxation rate that varies approximately linearly with Q, supports the idea that the PSEBS-in-PS L_3 phase becomes jammed on cooling to 120°C.

How could jamming occur in this case? Beyond Ref. [Milner et al.(1990)Milner, Cates, and Rou several experiments indicate that topological relaxations can be very slow in the L_3 phase [Waton and Porte(1993), Schwarz et al.(2000)Schwarz, Monch, Ilgenfritz, and Strey, Porcar et al.(2004)Porcar, Hamilton, Butler, and Warr], and in the analogous bicontinuous microemulsion phase [Peter et al.(2001)Peter, Roux, and Sood]. Therefore, we propose that the origin of jamming in the present case involves arrest of topological relaxation. Specifically, we hypothesize that, although the static structure is similar at the different temperatures studied, nevertheless changing the temperature causes the equilibrium topology to vary, for example, by changing slightly the equilibrium mean separation between membranes and the equilibrium thickness of the membrane. We further hypothesize that, for 140°C and above, the membrane topology is able to equilibrate, but that, because topological equilibration is activated and hence increasingly slow at lower temperatures and because collective diffusion is itself slowed because of the increased PS viscosity, at 120°C, the membrane topology does not equilibrate within the duration of the experiment. Under this constraint, the sponge structure will be subject to internal stresses associated with its topological frustration. Specifically, there will be a free energy cost per unit area associated with the deficit/surplus of membrane necks, *i.e.* the membrane will acquire a surface tension. Acccording to this interpretation, the deformations that occur as a result of these internal stresses, are then the origin of the relaxation of the ISF observed at 120°C, following Refs. [Cipelletti et al.(2000)Cipelletti, Manley, Ball, and Weitz, Cipelletti et al.(2003)Cipelletti, Ramos, Bandyopadhyay et al.(2004)Bandyopadhyay, Liang, Yardimci, Sessoms, Borthwick, Mochrie, Hard

BIBLIOGRAPHY

[Strey et al.(1990)Strey, Shomaker, Doux, Nallet, and Olsson] R. Strey, R. Shomaker, D. Doux, F. Nallet, and U. Olsson. *J. Chem. Soc., Faraday Trans.*, 86:2253, 1990.

[Roux et al.(1992)Roux, Coulon, and Cates] D. Roux, C. Coulon, and M. E. Cates. Sponge phases in surfactant solutions. *J. Phys. Chem.*, 96:4174–4187, 1992.

[Hillmyer et al.(1999)Hillmyer, Maurer, Lodge, Bates, and Almdal] M. A. Hillmyer, W. W. Maurer, T. P. Lodge, F. S. Bates, and K. Almdal. Model bicontinuous microemulsions in ternary homopolymer/block copolymer blends. *J. Phys. Chem. B*, 103:4814, 1999.

[Safinya et al.(1986)Safinya, Roux, Smith, Sinha, Dimon, Clark, and Bellocq] C. R. Safinya, D. Roux, G. S. Smith, S. K. Sinha, P. Dimon, N. A. Clark, and A. M. Bellocq. Steric repulsion in a lyotropic smectic liquid crystal. *Phys. Rev. Lett.*, 57:2718, 1986.

[Sikharulidze et al.(2002)Sikharulidze, Dolbnya, Fera, Madsen, Ostrovskii, and de Jeu] I. Sikharulidze, I. P. Dolbnya, A. Fera, A. Madsen, B. I. Ostrovskii, and W. H. de Jeu. Smectic membranes in motion: Approaching the fast limits of x-ray photon correlation spectroscopy. *Phys. Rev. Lett.*, 88: 115503, 2002.

[Helfrich(1973)] W. Helfrich. Elastic properties of lipid bilayers: theory and possible experiments. *Z. Naturforsch*, 28a:693, 1973.

[Morse(1994)] D. C. Morse. Topological instabilities and phase behavior of fluid membranes. *Phys. Rev. E*, 50:R2423, 1994.

[Golubovic(1994)] L. Golubovic. Passages and droplets in lamellar fluid phases. *Phys. Rev. E*, 50:R2419, 1994.

[Huang et al.(1987)Huang, Milner, Farago, and Richter] J. S. Huang, S. T. Milner, B. Farago, and D. Richter. Study of dynamics of microemulsion droplets by neutron spin echo spectroscopy. *Phys. Rev. Lett.*, 59:2600, 1987.

[Farago et al.(1990)Farago, Richter, Huang, Safran, and Milner] B. Farago, D. Richter, J. S. Huang, S. A. Safran, and S. T. Milner. Shape and size fluctuations of microemulsion droplets: The role of cosurfactant. *Phys. Rev. Lett.*, 65:3348, 1990.

[Milner and Safran(1987)] S. T. Milner and S. A. Safran. Shape fluctuations of microemulsion droplets. *Phys. Rev. A*, 36:4371, 1987.

[Cates et al.(1988)Cates, Roux, Andelman, Milner, and Safran] M. E. Cates, D. Roux, D. Andelman, S. T. Milner, and S. A. Safran. Random surface model for the l_3-phase of dilute surfactant solutions. *Europhys. Lett.*, 5:733, 1988.

[Blume et al.(1971)Blume, Emery, and Griffiths] M. Blume, V. J. Emery, and R. B. Griffiths. Ising model of the λ transition and phase separation in he^3-he^4 mixtures. *Phys. Rev. A*, 4:1071, 1971.

[Roux et al.(1990)Roux, Cates, Olsson, Ball, Nallet, and Bellocq] D. Roux, M. E. Cates, U. Olsson, R. C. Ball, F. Nallet, and A. M. Bellocq. Light scattering from a surfactant sponge phase: Evidence for a hidden symmetry. *Europhys. Lett.*, 9:229, 1990.

[Falus et al.(2004)Falus, Xiang, Borthwick, Russell, and Mochrie] P. Falus, H. Xiang, M. A. Borthwick, T. P. Russell, and S. G. J. Mochrie. Symmetric-to-asymmetric transition in triblock copolymer-homopolymer blends. *Phys. Rev. Lett.*, 93:145701, 2004.

[Gompper and Schick(1994)] G. Gompper and M. Schick. Scattering from internal interfaces in microemulsion and sponge phases. *Phys. Rev. E*, 49:1478, 1994.

[Frey and Nelson(1991)] E. Frey and D. R. Nelson. Dyanmics of flat membranes and flickering in red-blood-cells. *J. Phys. France I*, 1:1715, 1991.

[Zilman and Granek(1996)] A. G. Zilman and R. Granek. Undulations and dynamic structure factor of membranes. *Phys. Rev. Lett.*, 77:4788, 1996.

[Zilman and Granek(2002)] A. G. Zilman and R. Granek. Membrane dynamics and structure factor. *Chem. Phys.*, 284:195, 2002.

[Falus et al.(2005)Falus, Borthwick, and Mochrie] P. Falus, M. A. Borthwick, and S. G. J. Mochrie. Fluctuation dynamics of block copolymer vesicles. *Phys. Rev. Lett.*, 94:016105, 2005.

[Fox and Flory(1950)] T. G. Fox and P. J. Flory. Second-order transition temperatures and related properties of polystyrene. i. influence of molecular weight. *J. App. Phys.*, 21:581, 1950.

[Plazek and O'Rourke(1971)] D. J. Plazek and V. M. O'Rourke. Viscoelastic behavior of low molecular weight polystyrene. *J. Poly. Sci. Part A-2*, 9: 209, 1971.

[Freyssingeas et al.(1997)Freyssingeas, Roux, and Nallet] E. Freyssingeas, D. Roux, and F. Nallet. Quasielastic light scattering study of highly swollen lamellar and sponge phases. *J. de Physique II*, 7:913–929, 1997.

[Mihailescu et al.(2001)Mihailescu, Monkenbusch, Endo, Allgaier, Gompper, Stellbrink, Richter, J
M. Mihailescu, M. Monkenbusch, H. Endo, J. Allgaier, G. Gompper, J. Stellbrink, D. Richter, B. Jakobs, T. Sottmann, and B. Farago. Dynamics of bicontinuous microemulsion phases with and without amphiphilic block-copolymers. *J. Chem. Phys.*, 115:9563, 2001.

[Milner et al.(1990)Milner, Cates, and Roux] S. T. Milner, M. E. Cates, and D. Roux. Hydrodynamic modes and topology in microemulsion and l3 phases. *J. Physique*, 51:2629, 1990.

[Porte et al.(1991)Porte, Delsanti, Billard, Skouri, Appell, Marignan, and Debeauvais] G. Porte, M. Delsanti, I. Billard, M. Skouri, J. Appell, J. Marignan, and F. Debeauvais. Scaling laws for some physical properties of the l_3 (sponge) phase. *J. Phys. II France*, 1:1101, 1991.

[Granek and Cates(1992)] R. Granek and M. E. Cates. Sponge phase of surfactant solutions: An unusual dynamic structure factor. *Phys. Rev. A*, 46:3319, 1992.

[Waton and Porte(1993)] G. Waton and G. Porte. Transient behavior and relaxations of the l_3 (sponge) phase: T-jump experiments. *J. Phys II France*, 3:515, 1993.

[Gompper and Hennes(1994)] G. Gompper and M. Hennes. Equilibrium dynamics of microemulsion and sponge phases. *J. Phys II France*, 4:1375, 1994.

[Hennes and Gompper(1996)] M. Hennes and G. Gompper. Dynamical behavior of microemulsion and sponge phases in thermal equilibrium. *Phys. Rev. E*, 54:3811, 1996.

[Freyssingeas et al.(1996)Freyssingeas, Nallet, and Roux] E. Freyssingeas, F. Nallet, and D. Roux. Measurement of the membrane flexibility in lamellar and sponge phases of the c12e5/hexanol/water system. *Langmuir*, 12:6028, 1996.

[Nonomura and Ohta(1999)] M. Nonomura and T. Ohta. Decay rate of concentration fluctuations in microemulsions. *J. Chem. Phys.*, 110:7516, 1999.

[Schwarz et al.(2000)Schwarz, Monch, Ilgenfritz, and Strey] B. Schwarz, G. Monch, G. Ilgenfritz, and R. Strey. Dynamics of the sponge (l3) phase. *Langmuir*, 16:8643, 2000.

[Komura et al.(2001)Komura, Takeda, Kawabata, Ghosh, Seto, and Nagao] S. Komura, T. Takeda, Y. Kawabata, S. K. Ghosh, H. Seto, and M. Nagao. Dynamical fluctuation of the mesoscopic structure in ternary c12e5-water-n-octane amphiphile system. *Phys. Rev. E*, 63:041402, 2001.

[Holderer et al.(2005)Holderer, Frielinghaus, Byelov, Monkenbusch, Allgaier, and Richter] O. Holderer, H. Frielinghaus, D. Byelov, M. Monkenbusch, J. Allgaier, and D. Richter. Dynamic properties of microemuslions modified with homopolymers and diblock copolymers: The determination of bending moduli and renormalization effects. *J. Chem. Phys.*, 122:094908, 2005.

[Liu and Nagel(1998)] A. J. Liu and S. R. Nagel. Non-linear dynamics: Jamming is not just cool anymore. *Nature*, 396:21, 1998.

[Cipelletti et al.(2000)Cipelletti, Manley, Ball, and Weitz] L. Cipelletti, S. Manley, R. C. Ball, and D. A. Weitz. Universal aging features in the restructuring of fractal colloidal gels. *Phys. Rev. Lett.*, 84:2275 – 2278, 2000.

[O'Hern et al.(2001)O'Hern, Langer, Liu, and Nagel] C. S. O'Hern, S. A. Langer, A. J. Liu, and S. R. Nagel. Force distributions near jamming and glass transitions. *Phys. Rev. Lett.*, 86:111, 2001.

[Bandyopadhyay et al.(2004)Bandyopadhyay, Liang, Yardimci, Sessoms, Borthwick, Mochrie, Harc R. Bandyopadhyay, D. Liang, H. Yardimci, D. A. Sessoms, M. A. Borthwick, S. G. J. Mochrie, J. L. Harden, and R. L. Leheny. Evolution of particle-scale dynamics in an aging clay suspension. *Phys. Rev. Lett.*, 93:228302, 2004.

[Trappe et al.(2001)Trappe, Prassad, Cipelletti, Segre, and Weitz] V. Trappe, V. Prassad, L. Cipelletti, P. N. Segre, and D. A. Weitz. Jamming phase diagram for attractive particles. *Nature*, 411:772, 2001.

[Pham et al.(2002)Pham, Puertas, Bergenholtz, Egelhaaf, Moussaid, Pusey, Schofield, Cates, Fuch P. N. Pham, A. M. Puertas, J. Bergenholtz, S. U. Egelhaaf, A. Moussaid, P. N. Pusey, A. B. Schofield, M. E. Cates, M. Fuchs, and W. C. K. Poon. Multiple glassy states in a simple model system. *Science*, 296: 104, 2002.

[Bellour et al.(2003)Bellour, Knaebel, Harden, Lequeux, and Munch] M. Bellour, A. Knaebel, J. L. Harden, F. Lequeux, and J.-P. Munch. Aging processes and scale dependence in soft glassy colloidal suspensions. *Phys. Rev. E*, 67:031405, 2003.

[Cipelletti et al.(2003)Cipelletti, Ramos, Manley, Pitard, Weitz, Pashkovski, and Johansson] L. Cipelletti, L. Ramos, S. Manley, E. Pitard, D. A. Weitz, E. E. Pashkovski, and M. Johansson. Universal non-diffusive slow dynamics in aging soft matter. *Faraday Discuss.*, 123:237, 2003.

[Bouchard and Pitard(2001)] J.-P. Bouchard and E. Pitard. Anomalous dynamical light scattering in soft glassy gels. *Eur. Phys. J. E*, 6:231–236, 2001.

[de Gennes(1956)] P. G. de Gennes. Liquid dynamics and inelastic scattering of neutrons. *Physica*, 25:825–839, 1956.

[Porcar et al.(2004)Porcar, Hamilton, Butler, and Warr] L. Porcar, W. A. Hamilton, P. D. Butler, and G.G. Warr. Topological relaxation of a shear-induced lamellar to sponge equilibrium and the energetics of membrane fusion. *Phys. Rev. Lett.*, 93:198301, 2004.

[Peter et al.(2001)Peter, Roux, and Sood] U. Peter, D. Roux, and A. K. Sood. Observation of a topological relaxation mode in microemulsions. *Phys. Rev. Lett.*, 86:3340, 2001.

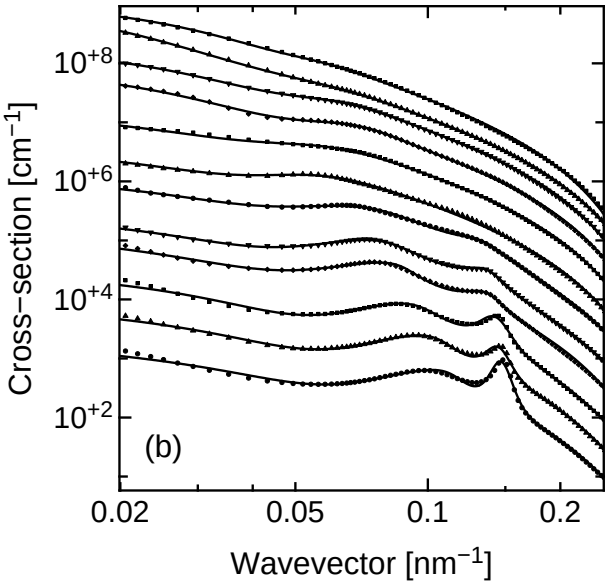

Figure 20: X-ray scattering cross-sections for PSEBS-PS blends *vs.* wavevector. Data for $\phi = 0.07$, 0.11, 0.15, 0.17, 0.19 in the vesicle phase and for $\phi = 0.22$, 0.25, 0.28, 0.31, 0.34, 0.37, 0.40 and 0.43 in the sponge phase plotted from 0.02 to 0.2 nm^{-1} on a log-log scale. These profiles have been multiplied by 3^{12}, 3^{11}, 3^{10}, 3^9, 3^8, 3^7, 3^6, 3^5, 3^4, 3^3, 3^2, 3, and 1, respectively. Solid lines correspond to the model discussed in the text. The dashed line through the profile for $\phi = 0.22$ corresponds to coexistence of 40% $\phi = 0.25$-volume fraction material with 60% $\phi = 0.19$-volume fraction material. The sharp peak that appears at larger volume fractions corresponds to the lamellar phase.

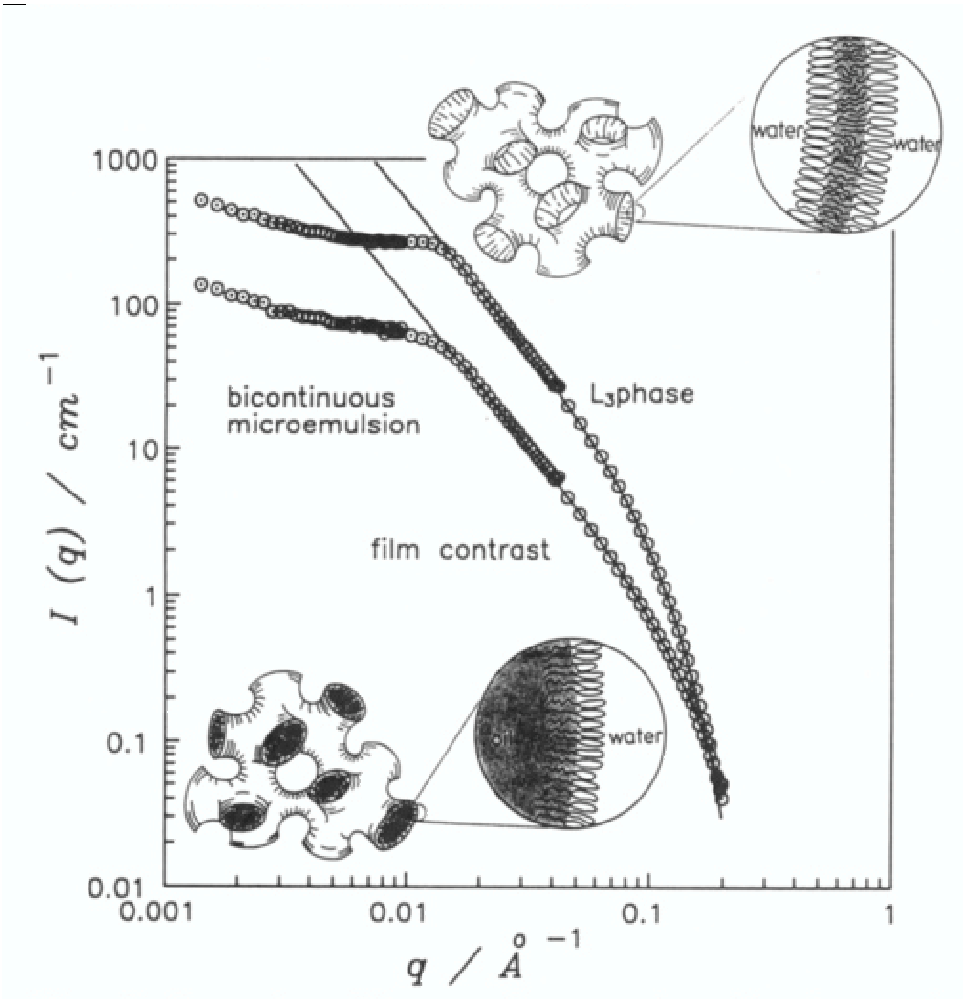

Figure 21: Comparison of the SANS profiles for, on the one hand, a sponge phase (top curve) and, on the other a BμE phase (bottom curve), studied in film contrast, so that the oil and water have essentially identical scattering length densities, which is very different from the scattering length density of the monolayer that separates the oil and water.

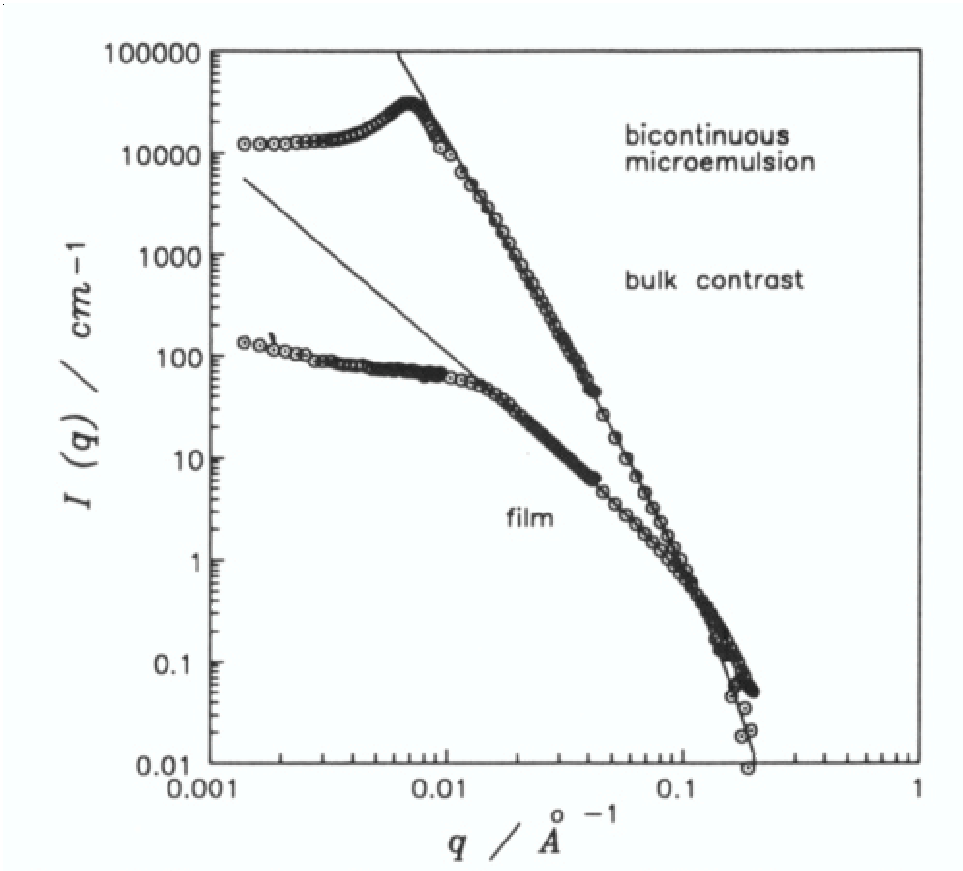

Figure 22: Comparison of the SANS profiles for a BμE phase, obtained, on the one hand, under film constrast (lower curve) and, on the other hand under bulk contrast (upper curve).

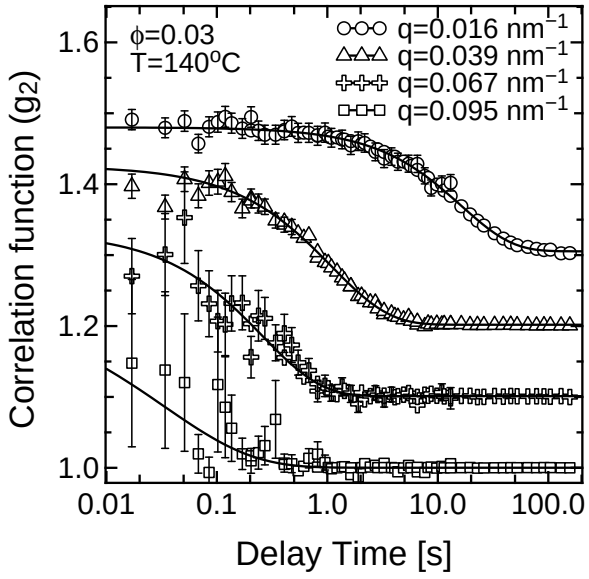

Figure 23: Intensity autocorrelation functions (g_2) *vs.* delay time at 140°C for wavevectors of 0.016 nm^{-1} (open circles), 0.039 nm^{-1} (open triangles), 0.067 nm^{-1} (open crosses), and 0.095 nm^{-1} (open squares). The solid lines correspond to least-squares fits to a stretched exponential form for the ISF. For clarity the curves have been shifted by 0.1 from each other.

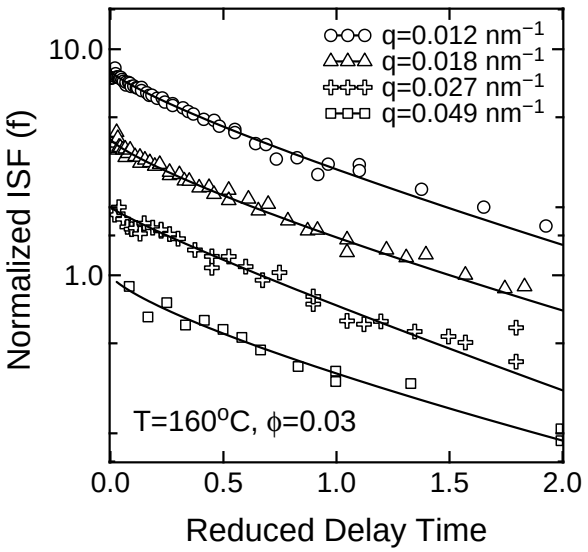

Figure 24: Normalized intermediate scattering functions [f] plotted *vs.* reduced delay time (Γt) at 160°C for wavevectors of 0.012 nm^{-1} (open circles), 0.018 nm^{-1} (open triangles), 0.027 nm^{-1} (open crosses), and 0.049 nm^{-1} (open squares), plotted on a logarithmic intensity scale and a linear reduced-delay-time scale. The solid lines are a stretched-exponential form, as discussed in the text. a single exponential fit would be a straight line. The solid curves are stretched exponential fits clearly deviating from straight lines. For clarity, data and model have been multiplied 8, 4, 2, 1 for wavevectors of 0.012 nm^{-1}, 0.018 nm^{-1}, 0.027 nm^{-1}, and 0.049 nm^{-1}, respectively.

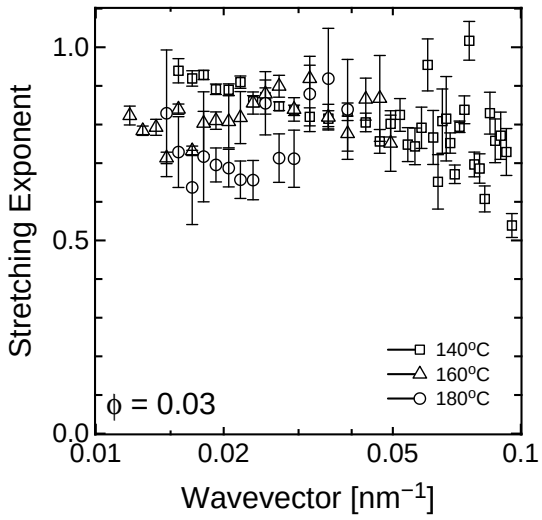

Figure 25: Stretching exponents for the $\phi = 0.03$-sample, for 180°C (open squares), 160°C (open crosses), and 140°C (open triangles).

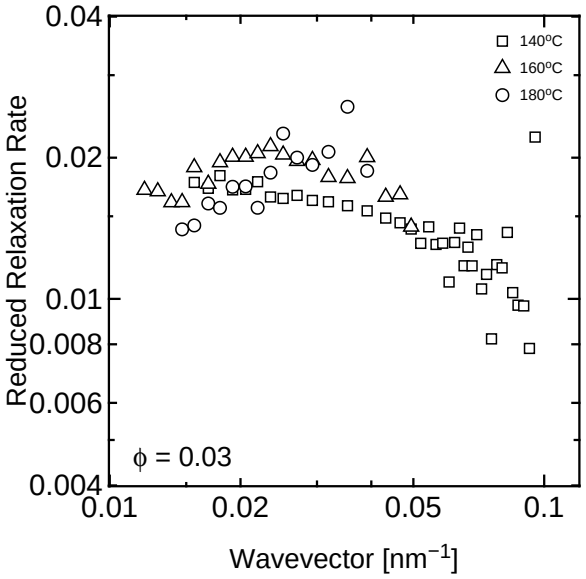

Figure 26: Reduced relaxation rate [$\tilde{\Gamma} = \Gamma\eta/(k_B T Q^3)$] of the 0.03-copolymer-volume-fraction for 180°C (open squares), 160°C (open crosses), and 140°C (open triangles), determined from stretched-exponential fits.

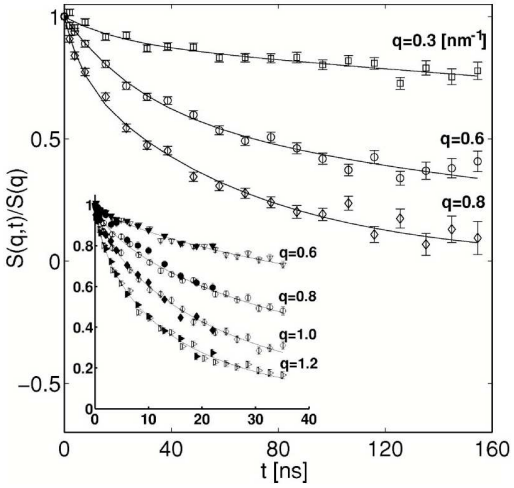

Figure 27: Measurements of the normalized ISF of water-decane-$C_{10}E_4$. Open symbols are ILL data. Solid symbols are Julich data. The solid lines are fits to a stretched exponential form, with Γ and β as fitting parameters.

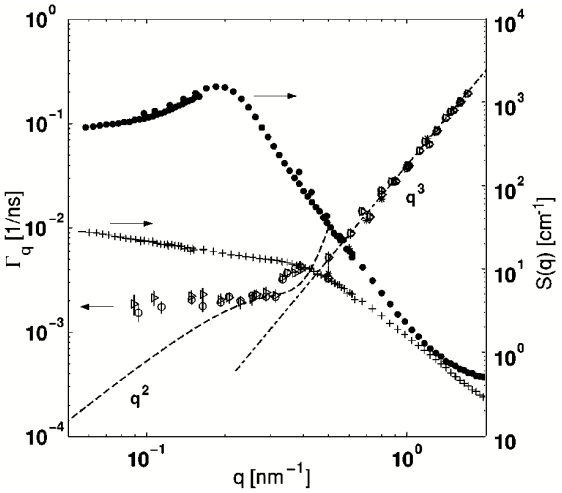

Figure 28: Summary of the relaxation rates, Γ_Q, *vs.* Q, obtained in film contrast for water-oil-$C_{10}E_4$ with (open triangles) and without (open circles) added PEP_{10}-PEO_{10} cosurfactant. At large Q, these results correspond to stretched exponential fits with $\beta \simeq 2/3$, as predicted. At small Q, single exponential fits were used, in part, because rates of about 1 MHz are at the limit of what is possible to measure with NSE. Also shown are the scattering intensities under bulk and film contrast.

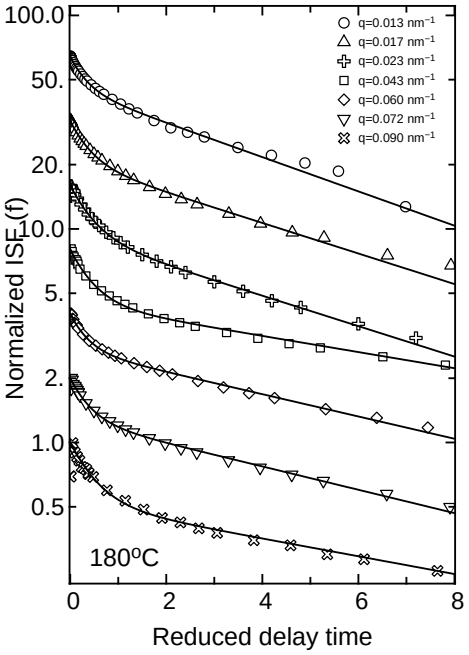

Figure 29: ISFs (f) *vs.* reduced delay time ($\Gamma_I t$) for several wavevectors at 180°C. For clarity, successive ISFs have been multiplied by factors of 1, 2, 4, 8, 16, 32, and 64, respectively. Solid lines are best-fits to a double-exponential form for the ISF.

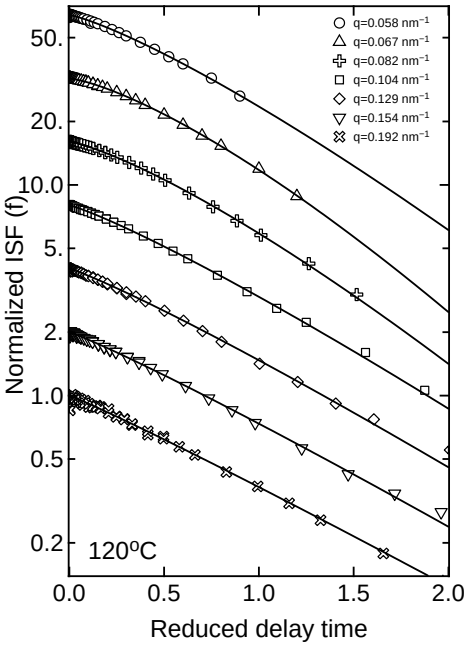

Figure 30: ISFs (f) *vs.* reduced delay time (Γt) for several wavevectors at 120°C. For clarity, successive ISFs have been multiplied by factors of 1, 2, 4, 8, 16, 32, and 64, respectively. Solid lines are the best fits to a stretched/compressed form for the ISF.

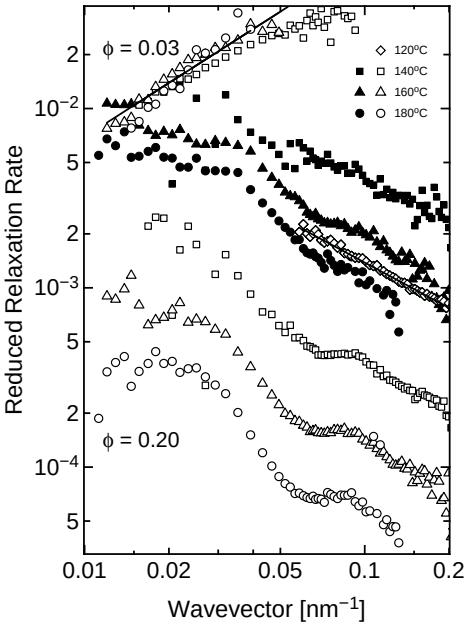

Figure 31: Reduced relaxation rate *vs.* Q. At 120°C, the open diamonds correspond to the Γs from stretched-exponential fits. At 140, 160, and 180°C, respectively, the solid aquares, triangles, and circles correspond to the fast mode (Γ_F), while the open squares, triangles, and circles correspond to the slow mode (Γ_S), as determined from double-exponential fits. The solid line through the 120°C-data corresponds to a $Q^{1.16}$-variation of the relaxation rate. Also shown are the relaxation rates from Ref. [Falus et al.(2004)Falus, Xiang, Borthwick, Russell, and Mochrie] obtained at 140°C, 160°C and 180°C for a PSEBS volume fraction of $\phi = 0.03$. The line through these data corresponds to the theoretical prediction of Ref. [Zilman and Granek(1996)].

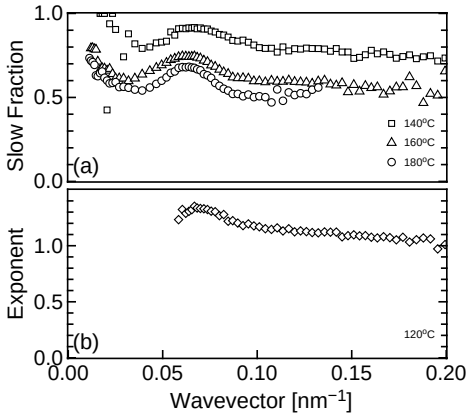

Figure 32: (a) Best-fit relative ampltude of the slow relaxation (a_S) *vs.* Q from fits using a double-exponential form for the ISF at 140°C (squares), 160°C (triangles), and 180°C (circles). (b) Best-fit stretching/compression exponent from fits using a stretched/compressed-exponential form for the ISF.